Observation of Superfluid Flow in a Bose-Einstein Condensed Gas

R. Onofrio, C. Raman, J. M. Vogels, J. R. Abo-Shaeer, A. P. Chikkatur, and W. Ketterle
Department of Physics and Research Laboratory of Electronics, Massachusetts Institute of Technology, Cambridge, Massachusetts 02139
(Received 5 June 2000)

We have studied the hydrodynamic flow in a Bose-Einstein condensate stirred by a macroscopic object, a blue-detuned laser beam, using nondestructive *in situ* phase contrast imaging. A critical velocity for the onset of a pressure gradient has been observed, and shown to be density dependent. The technique has been compared to a calorimetric method used previously to measure the heating induced by the motion of the laser beam.

PACS numbers: 03.75.Fi, 67.40.Vs, 67.57.De

Beginning with the London conjecture [1], Bose-Einstein condensation has been considered crucial for the understanding of superfluidity. Since then, the weakly interacting Bose gas has served as an idealized model for a superfluid [2]. It has a phononlike energy-momentum dispersion relation that does not allow for the generation of elementary excitations below a critical velocity, thus implying dissipationless flow. The onset of dissipation has been treated in the framework of the nonlinear Schrödinger equation [3–7] and shows an intriguing richness. Experiments on liquid helium could not test these theories, because superfluidity and dissipation are even more complex in this system due to the presence of strong interactions and surface effects [8].

The creation of Bose-Einstein condensates in dilute gases has dramatically changed this situation, allowing for quantitative tests of microscopic theories using the tools and precision of atomic physics experiments [9]. A number of recent experiments have examined phenomenological features of superfluidity in gaseous Bose-Einstein condensates. These include the observation of vortices [10,11], a nonclassical moment of inertia [12], and the suppression of collisions from microscopic impurities [13]. In previous work we found evidence for a critical velocity in a stirred condensate [14]. In this Letter we study the onset of dissipation with higher sensitivity using repeated *in situ* nondestructive imaging of the condensate. These images show the distortion of the density distribution around the moving object, thus directly probing the dynamics of the flow field that has been recently treated with different models [15–20].

The experimental setup was similar to the one used in our previous work [14]. Improvements in the evaporation strategy and decompression techniques allowed us to produce pure condensates with up to 5×10^7 sodium atoms, with densities ranging from 8.4×10^{13} to 3.5×10^{14} cm^{-3}, corresponding to chemical potentials from 60 to 250 nK. We determined the Thomas-Fermi radius R_z along the axial direction through *in situ* phase contrast imaging. The sound velocity at the center of the condensate was then evaluated through the relationship $c_s = 2\pi\nu_z R_z/\sqrt{2}$, with $\nu_z = 20.1$ Hz being the axial trapping frequency. The macroscopic moving object was a 514 nm laser beam blue-detuned with respect to the sodium transitions, thereby creating an effective repulsive potential for the atoms. The beam is focused on the center of the condensate to a Gaussian $1/e^2$ diameter of $2w = 10$ μm. It is scanned with an acousto-optic deflector driven by a triangular wave along the axial direction of confinement of the magnetic trap. This results in motion of the beam at a constant speed $v = 2af$, where f is the frequency and a is the amplitude of the scan. To avoid effects due to the inhomogeneous density distribution in the condensate, the laser was scanned at various frequencies with a constant amplitude approximately equal to the Thomas-Fermi radius R_z of the condensate along the axial direction.

The frequency range was limited to below 200 Hz. Above this frequency the atoms experience an effective time-averaged stationary potential. The condensate was imaged using the phase contrast technique [9,21] with probe light red-detuned from the $F = 1$ to $F' = 2$ transition. Different detunings (0.4 and 1.7 GHz) allowed us to maintain a large linear dynamic range when imaging condensates at different densities. Figure 1 shows multiple phase contrast images of the hydrodynamic evolution

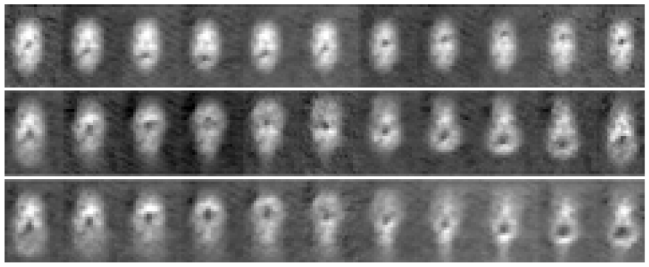

FIG. 1. Hydrodynamic flow in a Bose-Einstein condensate. Eleven phase contrast images of a condensate stirred for one cycle are taken *in situ* for various velocities of the laser beam. From top to bottom: 0.35, 5.6, and 9.0 mm/s. The exposure time is 300 μs per frame, and the frame rates are 33, 526, and 909 Hz, respectively. The maximum density and the corresponding sound velocity without the laser are 2×10^{14} cm^{-3} and 7 mm/s, respectively. The position of the laser beam is seen as a depletion of the condensate around its center. The vertical size of each image is $\simeq$200 μm.

 0031-9007/00/85(11)/2228(4)$15.00

of the density distribution of a single condensate during the stirring. For low velocities there was little effect on the condensate. However, at higher velocities the density distribution became asymmetrical and the condensate piled up in front of the moving beam, resulting in turbulent flow.

The main result of this Letter is based on quantitative analysis of images like those in Fig. 1. The observed flow pattern shows a critical velocity for the onset of a drag force between the laser beam and the condensate.

For a weakly interacting Bose-condensed gas at density $n(\mathbf{r})$ and chemical potential μ, pressure is identical to the mean-field energy density $P = \mu(\mathbf{r})n(\mathbf{r})/2$ [2]. A drag force arises due to the pressure difference across the moving object. The chemical potential is given by $\mu(\mathbf{r}, t) = gn(\mathbf{r}, t)$, where $g = 4\pi\hbar^2 a/M$ is the strength of two-body interactions for atoms with mass M and scattering length a. The drag force F is given by

$$F \simeq gSn\Delta n = S\mu\Delta\mu/g\,, \qquad (1)$$

where Δn and $\Delta\mu$ are the differences in density and chemical potential across the stirring object, and S the surface area the macroscopic object presents to the condensate. Equation (1) holds only for S much smaller than the condensate radial cross-sectional area.

If the laser beam is stationary, or moves slowly enough to preserve a possible superfluid state for the condensate, there will be no gradient in the chemical potential across the laser focus, and therefore zero force according to Eq. (1). A drag force between the moving beam and the condensate is indicated by an instantaneous density distribution $n(\mathbf{r}, t)$ that is distorted asymmetrically with respect to the laser beam. Figure 2 shows this asymmetry as the formation of a bow wave in front of and a stern wave behind the moving laser beam.

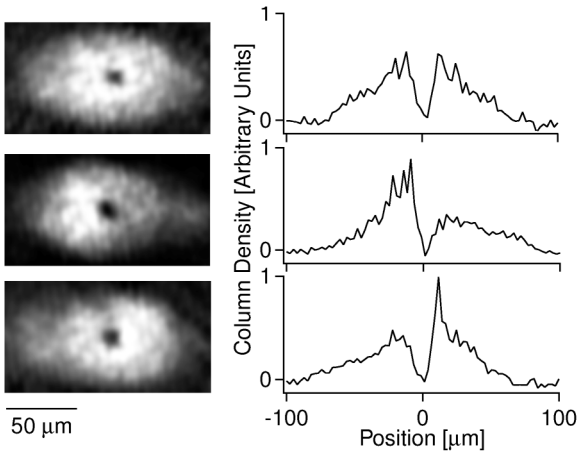

FIG. 2. Pressure difference across a laser beam moving through a condensate. On the left side *in situ* phase contrast images of the condensate are shown, strobed at each stirring half period: beam at rest (top), beam moving to the left (middle), and beam moving to the right (bottom). The profiles on the right are horizontal cuts through the center of the images. The stirring velocity and the maximum sound velocity were 3.0 and 6.5 mm/s, respectively.

To disentangle asymmetries due to the moving beam from the intrinsic inhomogeneity of the density profile we strobed the images at half the stirring period and always viewed the laser beam in the center of the condensate. We defined the asymmetry A as the relative difference between the peak column densities in front of ($\tilde{n}^f$) and behind ($\tilde{n}^b$) the laser beam $A = 2(\tilde{n}^f - \tilde{n}^b)/(\tilde{n}^f + \tilde{n}^b)$. We averaged A over nine successive images of the condensate.

The average asymmetry versus velocity is shown in Fig. 3. Below ~0.6 mm/s the asymmetry was zero within the statistical error indicating a suppression of dissipation in the superfluid regime. The asymmetry increased for velocities greater than 0.6 mm/s. The dip near 1.5 mm/s corresponds to a stirring frequency of ≃20 Hz for the chosen amplitude. This is close to the axial frequency of the magnetic trap. Near this frequency the laser beam synchronously excited the axial dipole motion of the condensate (see Fig. 3), thus reducing the *relative* velocity of the stirrer and the condensate and therefore the drag. We repeated the measurements at different stirring amplitudes to disentangle velocity and frequency dependent effects. This confirmed that the observed dip always occurred near 20 Hz, whereas the other features of the observed asymmetries depended only on velocity.

To study the superfluid regime at different atomic densities, we focused on the low velocity region ($v \leq 2$ mm/s) by choosing the stirring amplitudes in such a way that the

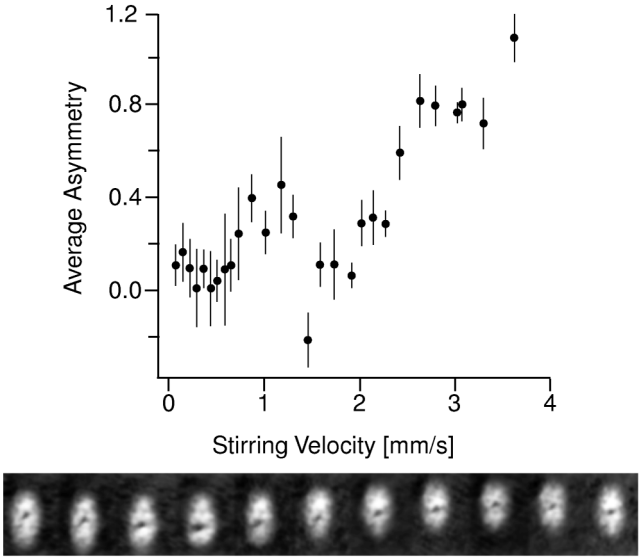

FIG. 3. Drag force on a Bose-Einstein condensate, derived as an asymmetry in the density profile (top). Beyond 4 mm/s the signal saturated due to the formation of a high-density bow wave, introducing nonlinearity into the phase contrast signal for phase shifts exceeding π. The bars represent statistical errors. Scanning the laser at the axial trapping frequency, corresponding to a stirring velocity of 1.5 mm/s for an amplitude of 37 μm, shows synchronous oscillations of the condensate (bottom) and reduced heating.

frequencies were below the trap resonance. The density was varied by adjusting the number of atoms for constant trapping parameters. The power in the laser beam was adjusted so that the potential height was 8 times the chemical potential (within 10%), thus preserving the effective size of the laser beam.

In Fig. 4 we show measurements of the average asymmetry for two maximum densities n_0 of 9×10^{13} and 1.9×10^{14} cm^{-3}. In each data set there is a threshold velocity v_c below which the drag force is negligible, and this threshold increases at higher density. Above this critical velocity, the drag force increases monotonically, with a larger slope at low density. The data were fitted to a piecewise linear function that reflects the two regimes of dissipation, one with zero asymmetry below v_c and another, above v_c, where the asymmetry is linear in $v - v_c$. The fits yield $v_c = (0.11 \pm 0.02)c_s$ for the higher density and $v_c = (0.07 \pm 0.02)c_s$ for the lower density. This is in agreement with the expectation that the critical velocity increases with the speed of sound and disagrees with models that predict only a dependence upon the diameter of the object [17,19].

One can compare measurements of the asymmetry (proportional to the drag force $\vec{F}$) with the rate of energy transferred to the condensate, $\vec{F} \cdot \vec{v}$, using an improved implementation of the calorimetric technique introduced in [14]. For this, we stirred the condensate for times between 100 ms and 8 s, in order to produce approximately the same final temperature. After the stirring beam was shut off, the cloud was allowed to equilibrate for 100 ms. The thermal fraction was determined using ballistic expansion and absorption imaging [9,14]. We inferred the temperature and total energy using the specific heat evaluated as in [22]. By comparing successive images with and without stirring of the condensate we subtracted out the residual background heating. As a result of the improved fitting and background subtraction procedure, we were able to detect changes of less than 10 nK in the energy of the gas, as we will describe in more detail in [23]. A condensed fraction higher than 90% ensured that the laser beam primarily heated the condensate and not the thermal cloud.

Figure 5 shows the energy transfer rate to the condensate versus the stirring velocity. Here, as in the phase contrast measurements, the amplitude of the stirring was kept fixed while scanning the frequency. We see the onset of dissipation near the value obtained using the drag force method, $v_c \simeq 0.5$ mm/s $= 0.1c_s$.

The calorimetric measurements can be compared with the drag force inferred from the asymmetric density distribution. Using Eq. (1), the energy transfer rate per atom is written in terms of the asymmetry as

$$\left.\frac{dE}{dt}\right|_{\text{asym}} \equiv \frac{\vec{F} \cdot \vec{v}}{N} \simeq \frac{8}{15} \frac{\mu_0 n_0 l_z d}{N} v A(v), \qquad (2)$$

where d is the diameter of the laser beam and l_z the Thomas-Fermi diameter in the radial direction.

The comparison between the calorimetric and the drag force measurements is also shown in Fig. 5. The heating inferred from the force measurement is in remarkable agreement with the calorimetric measurement over the entire velocity range up to a single scale factor for $vA(v)$, demonstrating the consistency between the two methods. For the parameters of our experiment ($d \simeq 10$ μm, $n_0 = 1.3 \times 10^{14}$ cm^{-3}, $l_z = 66$ μm, $N = 1.8 \times 10^7$) the overall heating rate predicted by Eq. (2) is 2.4 times larger than that obtained directly from calorimetry.

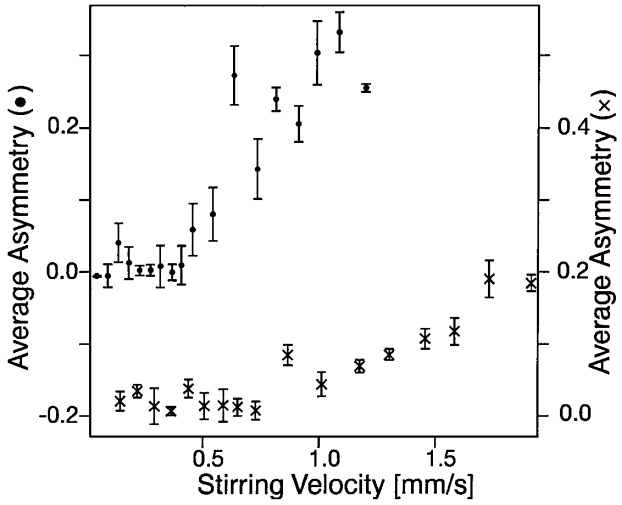

FIG. 4. Density dependence of the critical velocity. The onset of the drag force is shown for two different condensate densities, corresponding to maximum sound velocities of 4.8 mm/s (•, left axis) and 7.0 mm/s (×, right axis). The stirring amplitudes are 29 and 58 μm, respectively. The two vertical axes are offset for clarity. The bars represent statistical errors.

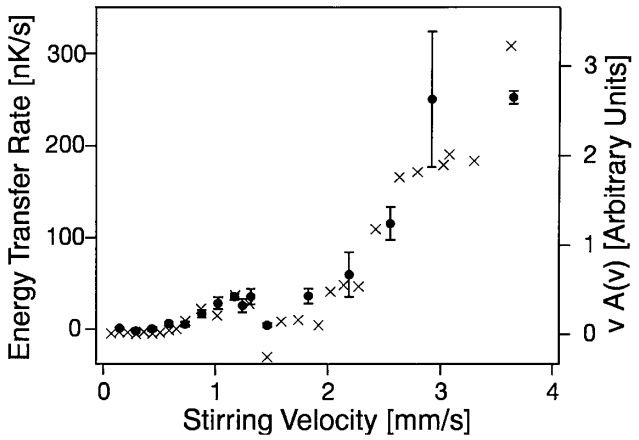

FIG. 5. Calorimetry of a condensate. The energy transfer rate during stirring (•, left axis) was obtained from temperature measurements. The error bars reflect shot-to-shot variations in the temperature. The results are compared to the energy transfer rate $vA(v)$ obtained from the asymmetry data of Fig. 3 (×, right axis).

Possible explanations for this difference are the inhomogeneous density profile or a breakdown of the quasistatic approximation embodied in Eqs. (1) and (2).

In one model [3], the drag force arises from the periodic emission of vortex lines at a rate that increases with velocity. The vortices reduce the pressure gradient across the object and the predicted heating rate is proportional to [3,6]

$$\left.\frac{dE}{dt}\right|_{\text{vortex}} \propto \frac{1}{N}\,\frac{\mu}{h}\,\frac{v}{c_s^2}\,(v - v_c)\epsilon_{\text{vortex}}\,, \qquad (3)$$

where $\epsilon_{\text{vortex}} = 2\pi\tilde{n}\hbar^2/M \ln(d/\xi)$ is the vortex energy and $\xi = (8\pi na)^{-1/2}$ is the healing length. Our observations are consistent with this model. Equations (2) and (3) predict that the slope of the asymmetry $\alpha = A(v)/(v - v_c)$ should scale as $\alpha \sim 1/c_s^2$. For the two densities in Fig. 4, the model predicts the ratio $\alpha_{\text{low}}/\alpha_{\text{high}} = 2.1$, while our measurement yields 1.9 ± 0.2. As a comparison, a kinetic model for the heating of a thermal cloud based on elastic collisions with a rigid wall implies $\alpha \sim 1/c$ [23], where c is now the thermal velocity $(2k_{\text{B}}T/M)^{1/2}$. In addition, the estimated heating rate due to vortex shedding is within a factor of 2 of the estimate in Eq. (3).

Our new measurements show that the critical velocity is smaller than estimated in our earlier experiment [14]. Both experiments are consistent, since the scatter in the observed heating rates in [14] prevented a clear observation of the threshold, and the critical velocity was determined by linear extrapolation from high heating rates to be $v_c/c_s = 0.25$. Other possible extrapolations tend to lower the value of v_c, for instance, a function $\propto v(v - v_c)$, as suggested by Eq. (2), yielded $v_c/c_s = 0.20 \pm 0.07$. With improved calorimetry we have taken data for parameters similar to [14] in the range $0.1 < v_c/c_s < 0.25$ and observed a small heating rate ($\simeq 20$ nK/s at 1 mm/s) that was previously indiscernible. Furthermore, small differences in the laser beam profile may have also contributed to the higher value of v_c in [14].

Since our first report on critical velocities in a condensate, several theoretical papers have added further insight [15–20]. The observed critical Mach number $v_c/c_s \simeq 0.1$ is lower than the predictions for homogeneous [3,5] and inhomogeneous [6] 2D systems. This discrepancy is most likely due to the actual 3D geometry, where the laser beam pierced lower density regions of the condensate. It was noted in Ref. [18] that the critical velocity for phonon excitation is lowered by the inhomogeneous density distribution. Vortex stretching and half-ring vortices can lower the 3D critical velocity below the 2D value [16]. Jackson *et al.* [15] performed 3D simulations obtaining a critical velocity as low as $0.13c_s$, quite close to our results. The relevant critical velocity is most likely related to vortex *nucleation* [3,5–7,15,16,19,20], which is usually smaller than the Landau and Feynman critical velocities [8] at which phonons [18] or vortices [17] become energetically favorable.

In conclusion, we have demonstrated a new technique to study dissipation in a stirred condensate. This method directly measures density distributions and pressure differences, and allows multiple nonperturbative images of the flow field. The flow pattern measurements may allow detailed comparison with contradictory predictions about the onset of dissipation in a gaseous superfluid [15–20].

We thank A. Görlitz, C. E. Kuklewicz, and Z. Hadzibabic for initial contributions to this experiment, and D. Kokorowski for a critical reading of the manuscript. This work has been supported by ONR, NSF, ARO, NASA, and the David and Lucile Packard Foundation. A. P. C. acknowledges additional support from NSF.

[1] F. London, Nature (London) **141**, 643 (1938).
[2] F. Dalfovo *et al.,* Rev. Mod. Phys. **71**, 463 (1999).
[3] T. Frisch, Y. Pomeau, and S. Rica, Phys. Rev. Lett. **69**, 1644 (1992).
[4] V. Hakim, Phys. Rev. E **55**, 2835 (1997).
[5] C. Huepe and M.-E. Brachet, C. R. Acad. Sci. Paris **325**, 195 (1997).
[6] T. Winiecki, J. F. McCann, and C. S. Adams, Phys. Rev. Lett. **82**, 5186 (1999).
[7] B. M. Caradoc-Davies, R. J. Ballagh, and K. Burnett, Phys. Rev. Lett. **83**, 895 (1999).
[8] J. Wilks and D. S. Betts, *An Introduction to Liquid Helium* (Clarendon Press, Oxford, 1987).
[9] For a review see *Bose-Einstein Condensation in Atomic Gases,* Proceedings of the International School of Physics "Enrico Fermi," edited by M. Inguscio, S. Stringari, and C. E. Wieman (IOS Press, Amsterdam, 1999).
[10] M. R. Matthews *et al.,* Phys. Rev. Lett. **83**, 2498 (1999).
[11] K. W. Madison *et al.,* Phys. Rev. Lett. **84**, 806 (2000).
[12] O. M. Maragò *et al.,* Phys. Rev. Lett. **84**, 2056 (2000).
[13] A. P. Chikkatur *et al.,* Phys. Rev. Lett. **85**, 483 (2000).
[14] C. Raman *et al.,* Phys. Rev. Lett. **83**, 2502 (1999).
[15] B. Jackson, J. F. McCann, and C. S. Adams, Phys. Rev. A **61**, 013604 (2000); **61**, 051603(R) (2000).
[16] C. Nore, C. Huepe, and M. E. Brachet, Phys. Rev. Lett. **84**, 2191 (2000).
[17] M. Crescimanno *et al.,* Phys. Rev. A (to be published).
[18] P. O. Fedichev and G. V. Shlyapnikov, e-print cond-mat/0004039.
[19] J. S. Stießberger and W. Zwerger (to be published).
[20] T. Winiecki *et al.,* e-print cond-mat/0004430.
[21] M. R. Andrews *et al.,* Science **273**, 84 (1996).
[22] S. Giorgini, L. P. Pitaevskii, and S. Stringari, J. Low Temp. Phys. **109**, 309 (1997).
[23] C. Raman *et al.* (to be published).